Chalcogenide Letters Vol. 20, No. 9, September 2023, p. 639 - 648

Rational design of MoS_2 nanosheet/ MoS_2 nanowire homostructures and their enhanced hydrogen evolution reaction

L. Yang*, X. Q. Yuan, R. Y. Liu, R. X. Song, Q. W. Wang, W. Liang
Key Laboratory of Biomimetic Sensor and Detecting Technology of Anhui Province, School of Materials and Chemical Engineering, West Anhui University, Luan, Anhui, 237012, P. R. China

In this paper, we report a facile method for the synthesis of MoS_2 nanosheet/ MoS_2 nanowire homostructures by growing MoS_2 nanosheets on the surface of MoS_2 nanowires. Benefiting from the uniform coating of MoS_2 nanosheets on the surface of MoS_2 nanowires, the MoS_2 nanosheet/ MoS_2 nanowire homostructures highly expose their electrocatalytic active edge sites and exhibit an enhanced electrocatalytic performance. It demonstrates a low overpotential of 107 mV at 10 mA/cm^2 and a small Tafel slope of 64 mV/dec in 0.5 M H_2SO_4. This work provides an inspiration for the design of efficient electrocatalysts with no stacking and aggregation structure.

(Received May 26, 2023; Accepted September 1, 2023)

Keywords: Transition metal chalcogenide, MoS_2 nanosheet/ MoS_2 nanowire homostructures, Electrocatalytic active edge sites, Coating structure, Hydrogen evolution reaction

1. Introduction

With the environmental pollution problem becoming more and more serious, it is urgent to find environment-friendly energy sources [1-3]. Hydrogen has attracted much attention in recent years because of its pollution-free combustion and high energy density (143 kJ/g) [4-6]. Among the ways to produce hydrogen, electrocatalytic hydrogen evolution reaction (HER) in water splitting has been regarded as an efficiency way to produce clean hydrogen energy [7]. At present, the noble metals like Pt exhibit the highest efficiency in electrocatalytic water splitting, but the limited reserve and high price highly restrict their large-scale application [8-10]. Therefore, exploring alternative catalysts with low price, high reserves, and excellent efficiency becomes urgent. Transition metal dichalcogenides (TMDs) represented by MoS_2, have attracted attraction due to their suitable Gibbs free energy for hydrogen absorption [11]. Theoretical calculations and experimental studies have shown that the edges of MoS_2 were electrochemical active, whereas the basal planes were inert [11-13]. Therefore, highly increasing and exposing the active edge sites are the efficiency way to enhance the electrocatalytic performance of MoS_2 [14-19]. In addition, the high electrocatalytic activities of MoS_2 edges mainly come from the unsaturated S atoms, therefore, forming amorphous structures and creating defective MoS_2 structures are often used to increase the

* Corresponding author: leiyang@wxc.edu.cn
https://doi.org/10.15251/CL.2023.209.639

active edge sites density [12, 20-22]. Lowing the dimension can increase the specific surface area of MoS_2, thus can also be used to increase the number of active sites [23,24]. Nanostructuring MoS_2 with various morphologies is another efficient way to enhance the HER performance, for example, MoS_2 with vertically aligned layers or double-gyroid morphologies can maximally expose the active edges on the surface [25,26]. For the structures prepared by hydrothermal method, the MoS_2 nanosheets often show a stacking structure. The stacking structure makes the nanosheets aggregate, which is not beneficial to expose the active edge sites [27-29]. Therefore the electrocatalytic performance of MoS_2 always be hampered. In this paper, MoS_2 nanowires are synthesized via electrospinning and subsequent sulfurization process by using sulfur and phosphomolybdic acid (PMA) as precursors. Then we grow MoS_2 nanosheets on the surface of MoS_2 nanowires by the hydrothermal method. X-ray diffraction (XRD), Scanning electron microscopy (SEM), transmission electron microscopy (TEM), X-ray Photoelectron Spectroscopy (XPS) and BET were utilized to characterize the as-synthesized MoS_2 nanosheet/ MoS_2 nanowire homostructures. Benefitting from the uniform coating structure, the aggregation is avoided and the active edges sites are maximally exposed. It delivers a low overpotential of 107 mV at 10 mA/cm^2 and a small Tafel slope of 64 mV/dec in acid media. It is expected to become an alternative to noble metal electrocatalysts in the future.

2. Experimental details

2.1. Synthesis of one dimensional (1D) MoS_2 nanowires

1D MoS_2 nanowires were synthesized by two steps. Firstly, electrospinning method was used to prepare PVP/PMA nanowires. 1.2 g PVP and 2 g PMA were dissolved in 10 mL N, N-Dimethylformamide (DMF). With continuous stirring for ~6 h, the solution became transparent. Then the transparent solution with no bubbles was transferred to syringe. The syringe pump with the rate of 0.8 mL/h was used to drive the solution. The voltage between the collector (aluminum foil) and the needle of syringe was set to 16 kV, and the distance was fixed at 15 cm. After electrospinning process, the as-electrospun PVP/PMA nanowires were dried at 80 ℃ for 12 h in air to stabilize their morphologies. Secondly, a sulfurization process was performed under an inert and reductive atmosphere to convert the 1D PVP/PMA nanowires into 1D MoS_2 nanowires. The as-dried 1D PVP/PMA nanowires and sulfur powder were placed on two aluminum oxide ceramic boat, respectively. The mass ratio of PVP/PMA nanowires to sulfur powder was 1:10. The ceramic boat loaded with PVP/PMA nanowires was placed at the center of the quartz tube furnace, and the sulfur powder was 13 cm upstream away from the PVP/PMA nanowires. During the sulfurization process, the quartz tube furnace was firstly heated to 200 ℃ and kept at 200 ℃ for 1 h. Then the furnace was heated to 900 ℃ and kept at 900 °C for 1 h. The mixture gas of Ar/H_2(5%) with the flow rate of 50 sccm was used as the carrier and reducing gas during the whole process. After the furnace cooled, 1D MoS_2 nanowires were successfully synthesized.

2.2. Synthesis of MoS_2 nanosheets

MoS_2 nanosheets were synthesized by the hydrothermal method. 0.08 g $(NH_4)_6Mo_7O_{24}\cdot 4H_2O$ and 0.16 g CH_4N_2S were dissolved in 40 mL deionized water. With continuous stirring for~1 h, the solution was transferred to the Teflon-lined stainless autoclave

with a capacity of 50 mL. The autoclave was heated at 200 ℃ for 12 h in the oven. After the reaction, the products were washed with distilled water and absolute ethanol to remove the impurities and then were dried in the vacuum oven to eliminate the adsorbate.

2.3. Synthesis of MoS_2 nanosheet/ MoS_2 nanowire homostructures

The procedures for the synthesis of MoS_2 nanosheet/ MoS_2 nanowire homostructures were similar to that of MoS_2 nanosheets. The difference was that 0.5 g MoS_2 nanowires prepared by electrospinning and subsequent sulfurization process were added to the Teflon-lined stainless autoclave during the hydrothermal process. With MoS_2 nanowires added to the reaction solution, they served as the substrates for the growth of MoS_2 nanosheets, thus forming the homogeneous structures of MoS_2 nanosheet/MoS_2 nanowire.

2.4. Electrocatalytic measurements

The electrocatalytic measurements of HER in water splitting of as-synthesized MoS_2 nanosheet/ MoS_2 nanowire homostructures were characterized in a CHI 660E electrochemistry workstation. The measurement was performed in the 0.5 mol/L H_2SO_4 solution. The procedures were published in our previous work [30].

3. Results and discussion

SEM was used to character the morphologies of as-synthesized MoS_2 nanosheets, MoS_2 nanowires and MoS_2 nanosheet/ MoS_2 nanowire homostructures. Figure 1(a) and 1(b) shows the SEM images of as-electrospun PVP/PMA nanowires. The nanowires show a smooth surface with the uniform diameter in the range of 100 nm-250 nm. Undergoing the sulfurization process, the PVP/PMA nanowires were completely converted into MoS_2 nanowires successfully, as depicted in Figure 1(c) and 1(d). The morphology of nanowires did not change before and after the sulfurization. Figure 1(e) and 1(f) display the SEM images of MoS_2 nanosheets synthesized by the hydrothermal method. The MoS_2 nanosheets show the aggregation morphology with nanoflower-like structure. The stacking structure restricts the exposure of active edge sites, which makes the HER performance be hampered, as discussed below. By using electrospinning, sulfurization followed by hydrothermal process, MoS_2 nanosheet/ MoS_2 nanowire homostructures were formed, as shown in Figure 1(g) and 1(h). The MoS_2 nanosheets are coated on the surface of MoS_2 nanowires with preferential c-parallel orientation. Compared with the pure MoS_2 nanosheets, the aggregation is effectively avoided, and the edges of MoS_2 nanosheets are highly exposed in the MoS_2 nanosheet/ MoS_2 nanowire homostructures. The successful synthesis of MoS_2 nanosheet/ MoS_2 nanowire homostructures indicates that the MoS_2 nanowires are the ideal substrates for the synthesis of MoS_2 nanosheets.

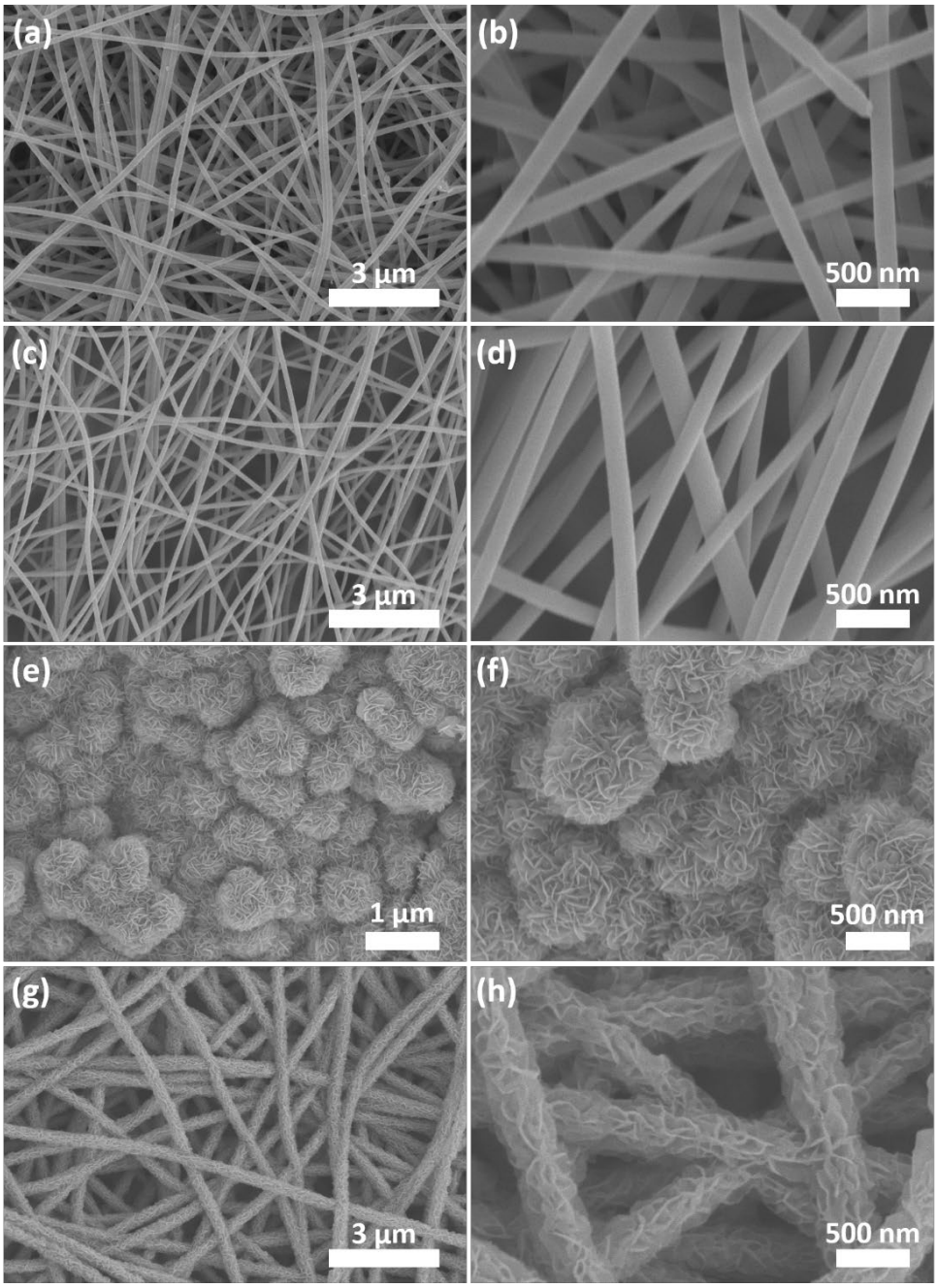

Fig. 1. (a) and (b) SEM images of as-electrospun PVP/PMA nanowires. (c) and (d) SEM images of as-synthesized MoS_2 nanowires. The diameter of the nanowires is in the range of 100 nm-250 nm. (e) and (f) SEM images of MoS_2 nanosheets. The nanosheets agglomerate to form nanoflower-like structure . (g) and (h) SEM images of as-synthesized MoS_2 nanosheet/ MoS_2 nanowire homostructures. The MoS_2 nanosheets were vertically standing on the surface of MoS_2 nanowires, and the active edge sites were highly exposed.

The crystal structure of as-synthesized samples was characterized by XRD, as shown in Figure 2(a). The XRD patterns of MoS_2 nanosheets, MoS_2 nanowires and MoS_2 nanosheet/ MoS_2 nanowire homostructures all exhibit obvious peaks at 14.1°, 33.6°, 39.6° and 58.8° which corresponds to the diffraction peaks of hexagonal MoS_2 with the JCPDS Card No. 37-1492 [31]. The peaks marked by * correspond to the diffraction peaks of the C which is produced by carbonization of PVP. Figure 2(b) shows the TEM image of MoS_2 nanosheet/ MoS_2 nanowire homostructures. It's obvious that the thin MoS_2 nanosheets are coated on the surface of MoS_2 nanowires, which is consistent with the results in SEM characterizations. The high resolution TEM (HRTEM) image of MoS_2 nanosheet/ MoS_2 nanowire homostructures is depicted in Figure 2(c). The clear lattice fringes indicate that the as-synthesized samples are well crystalline. The lattice spacing of 0.62 nm corresponds to the (002) adjacent layer spacing of MoS_2 [32]. To visualize the composition of as-synthesized sample, energy-dispersive X-ray (EDX) characterization was also performed, as exhibited in Figure 2(d). The EDX mapping clearly demonstrates that Mo and S atoms are the basic chemical composition of the as-synthesized MoS_2 nanosheet/ MoS_2 nanowire homostructures.

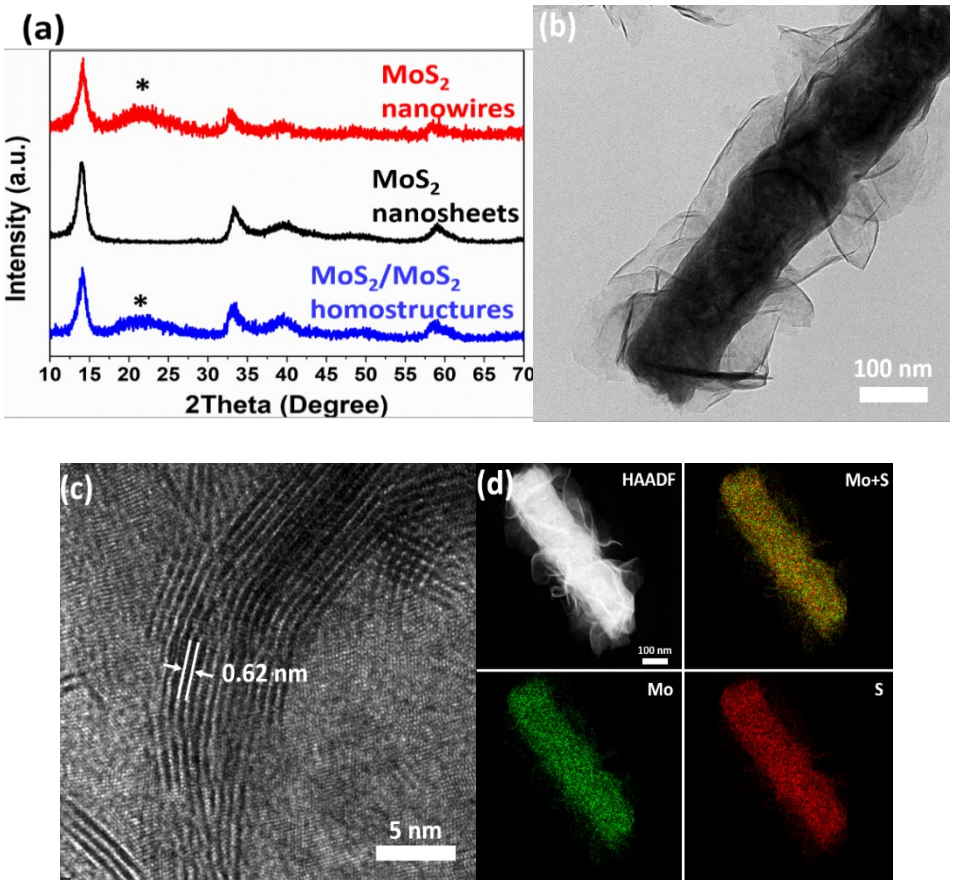

Fig. 2. (a) XRD patterns of as-synthesized MoS_2 nanosheets, MoS_2 nanowires and MoS_2 nanosheet/ MoS_2 nanowire homostructures. (b) TEM image of MoS_2 nanosheet/ MoS_2 nanowire homostructures. The MoS_2 nanosheets are coated on the surface of MoS_2 nanowires, and the active edge sites are highly exposed. (c) HRTEM image of as-synthesized MoS_2 nanosheet/ MoS_2 nanowire homostructures. The lattice fringes of 0.62 nm are indexed to the adjacent layer spacing of (002)

planes. (d) EDX mapping of MoS_2 nanosheet/ MoS_2 nanowire homostructures. It confirms the basic chemical composition of the sample.

The chemical composition of as-synthesized samples were further demonstrated by the XPS. The Mo 3d and S 2p orbital peaks are shown in Figure 3. The peaks located at ~226.9 eV correspond to the S 2s [33,34]. As for the Mo 3d, two obvious peaks located at 229.7 eV and 232.9 eV are attributed to the Mo^{4+} $3d_{5/2}$ and Mo^{4+} $3d_{5/2}$, respectively [33]. The binding energies of 162.5 eV and 163.6 eV are assigned to the S $2p_{3/2}$ and S $2p_{1/2}$ peaks, respectively [35].

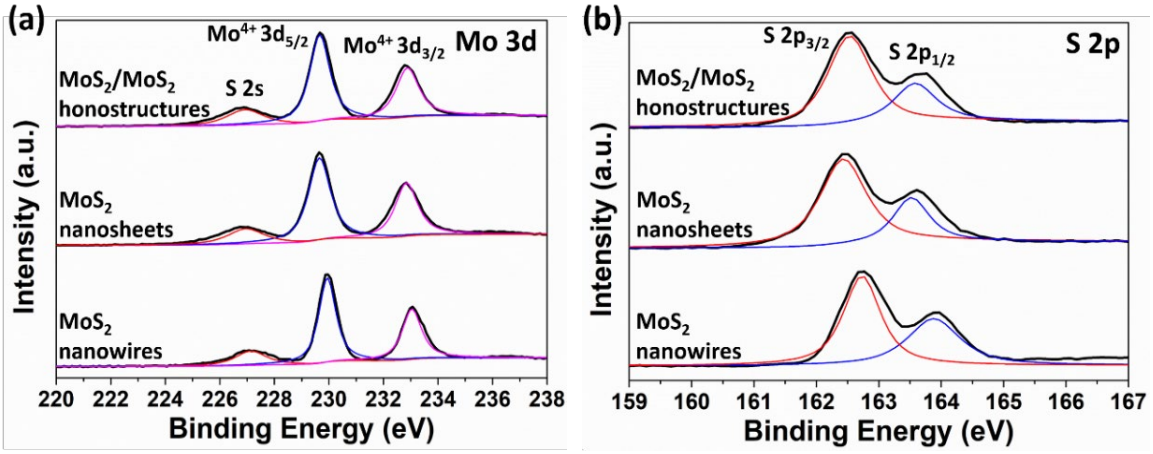

Fig. 3. XPS measurements for Mo and S binding energies in the as-synthesized MoS_2 nanosheets, MoS_2 nanowires and MoS_2 nanosheet/ MoS_2 nanowire homostructures.

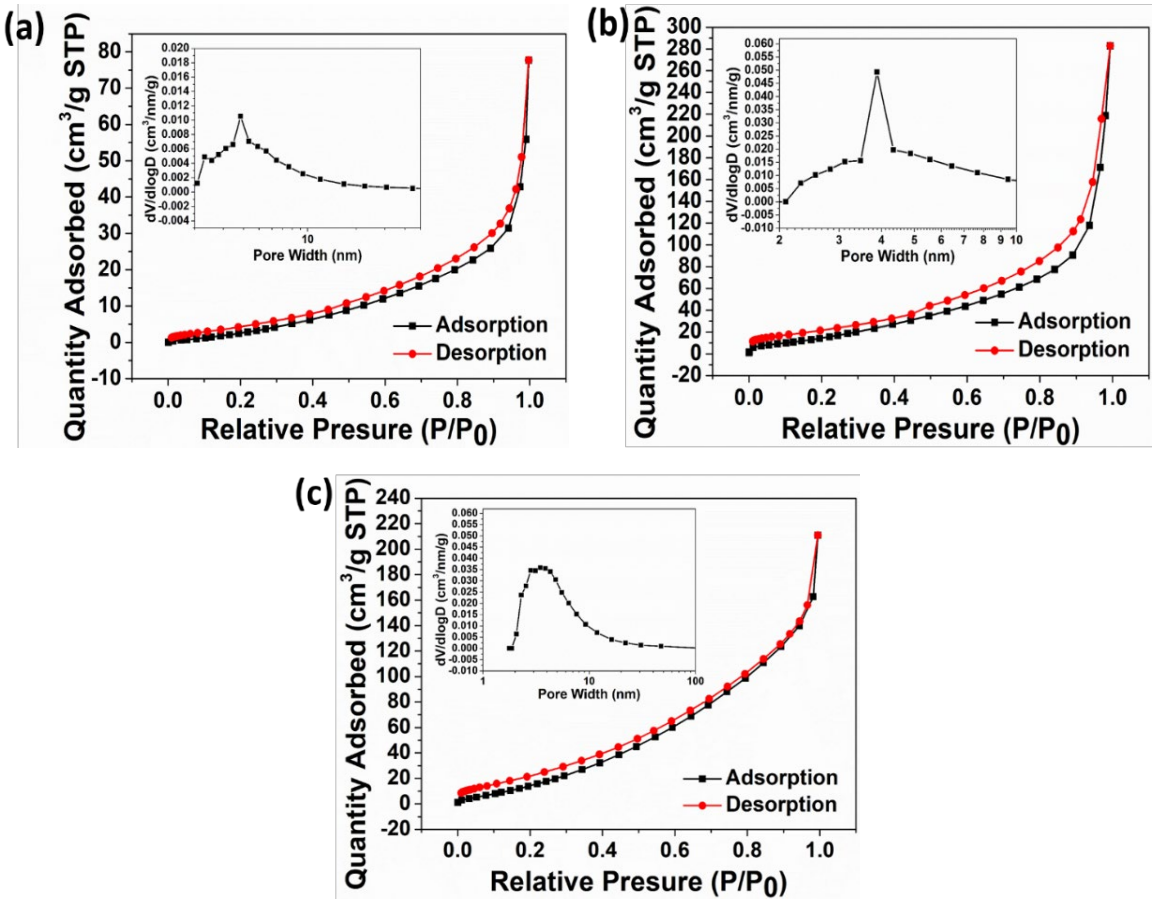

Fig. 4. N_2 adsorption/desorption isotherms and corresponding pore size distribution curves of (a) MoS_2 nanosheets, (b) MoS_2 nanowires, and (c) MoS_2 nanosheet/ MoS_2 nanowire homostructures.

The XPS results clearly show the existence of Mo and S elements in the as-prepared samples, which is in great agreement with the EDS mapping characterizations. As shown in Figure 4, the texture properties of the samples are characterized by the N_2 adsorption/desorption tests. The BET surface area of MoS_2 nanosheets and MoS_2 nanowires are 33.1 m^2/g and 89.1 m^2/g, respectively, which are smaller than that of MoS_2 nanosheet/ MoS_2 nanowire homostructures (143.1 m^2/g). The larger specific surface area indicates that the MoS_2 nanosheet/ MoS_2 nanowire homostructures expose more active edge sites for HER in water splitting. For the pore size of the samples, the MoS_2 nanosheet/ MoS_2 nanowire homostructures center at 3.4 nm, close to that of MoS_2 nanosheets (3.8 nm) and MoS_2 nanowires (3.9 nm), as shown in the insets of Figure 4.

The HER activities of as-synthesized samples were characterized using a three-electrode configuration in 0.5 M H_2SO_4. Figure 5(a) displays the HER polarization curves of MoS_2 nanowires, MoS_2 nanosheets and MoS_2 nanosheet/ MoS_2 nanowire homostructures. The overpotential of MoS_2 nanosheet/ MoS_2 nanowire homostructures at the current density of 10 mA/cm^2 is 107 mV, which is smaller than that of MoS_2 nanowires (170 mV) and MoS_2 nanosheets (163 mV). Furthermore, the current density observed in the MoS_2 nanosheet/ MoS_2 nanowire homostructures (245 mA/cm^2) is larger than that in MoS_2 nanowires (116 mA/cm^2) and MoS_2 nanosheets (131 mA/cm^2) at the overpotential of 400 mV. The larger current density implies that it's easy to transfer electrons between catalysts and electrode.

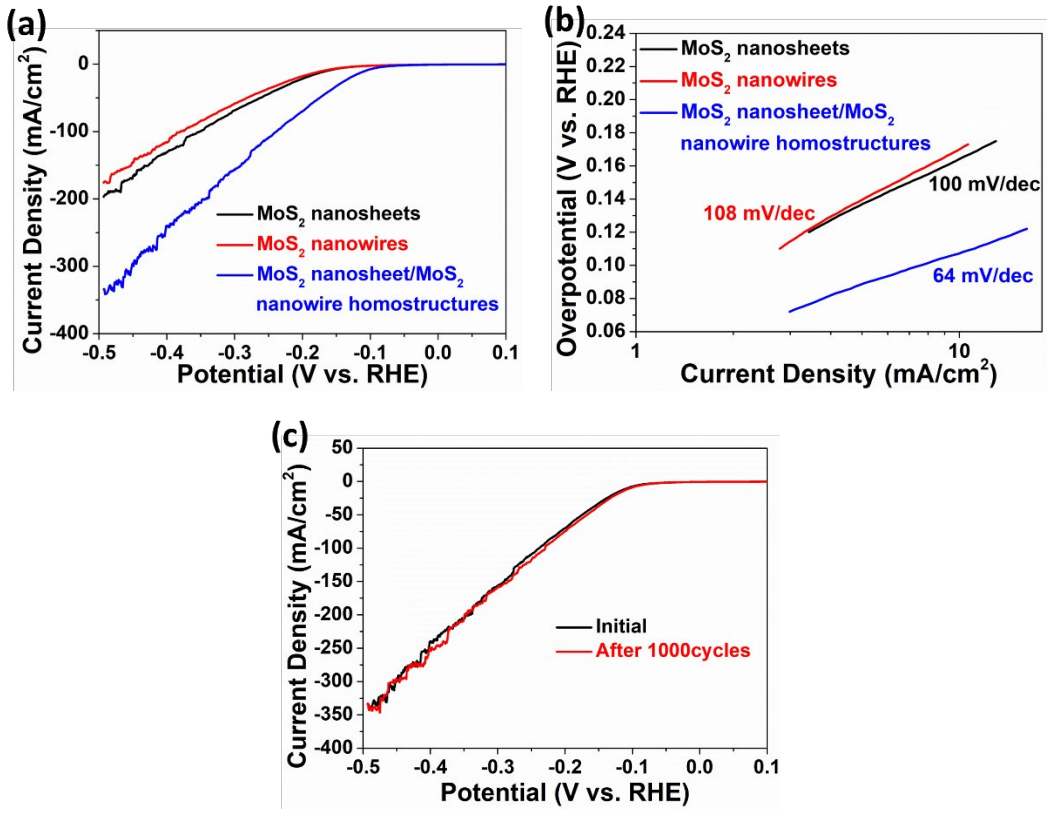

Fig. 5. (a) Polarization curves and (b) Tafel plots of as-synthesized MoS_2 nanowires, MoS_2 nanosheets and MoS_2 nanosheet/ MoS_2 nanowire homostructures in H_2SO_4. (c) Stability characterization of MoS_2 nanosheet/ MoS_2 nanowire homostructures.

Tafel slope is also an important parameter to assess the electrocatalytic activity of catalysts. As displayed in Figure 5(b), the Tafel slope of MoS_2 nanosheet/ MoS_2 nanowire homostructures (64 mV/dec) is clearly smaller than that of MoS_2 nanowires (108 mV/dec) and MoS_2 nanosheets (100 mV/dec). It indicates that the MoS_2 nanosheet/ MoS_2 nanowire homostructures possess faster HER kinetics during electrocatalytic water splitting. The polarization curves and Tafel slope characterizations manifest that the MoS_2 nanosheet/ MoS_2 nanowire homostructures exhibit enhanced HER performance compared to the MoS_2 nanosheets and MoS_2 nanowires. Besides, we also character the electrocatalytic stability during the HER process. As shown in Figure 5(c), the polarization curves almost coincide before and after 1000 cycles, which indicates that the MoS_2 nanosheet/ MoS_2 nanowire homostructures show an excellent elctrocatalytic stability.

For the MoS_2, the electrocatalytic inert basal planes always limit the HER performance. As shown in the SEM images, the MoS_2 nanosheets stacking together form a nanoflower-like morphology, which hides the active edge sites of MoS_2. Therefore, the MoS_2 nanosheets exhibit a hampered electrocatalytic performance. By growing MoS_2 nanosheets on the surface of MoS_2 nanowires, the active edge sites are highly exposed. As a result, the MoS_2 nanosheet/ MoS_2 nanowire homostructures exhibit a superior electrocatalytic performance.

4. Conclusions

In summary, we have synthesized MoS_2 nanosheet/ MoS_2 nanowire homostructures by using electrospinning, sulfurization followed by hydrothermal process. The MoS_2 nanosheets vertically standing on the surface of MoS_2 nanowires makes the MoS_2 active edge sites be highly exposed, and the aggregation effect be avoided. As a result, compared to MoS_2 nanosheets and MoS_2 nanowires, the MoS_2 nanosheet/ MoS_2 nanowire homostructures show enhanced electrocatalytic performance with the overpotential of 107 mV at the current density of 10 mA/cm^2, a Tafel slope of 64 mV /dec and excellent stability. Our results provide an efficient way to highly expose the HER active edge sites, which can be applied to other electrocatalysts system.

Acknowledgements

This work was supported by the National Natural Science Foundation of China (NSFC) (12104343), Excellent Youth Research Project of Education Department of Anhui Province (2022AH030148) and National college student innovation and entrepreneurship training program (202210376075).

References

[1] M. G. Walter, E. L. Warren, J. R. McKone, S. W. Boettcher, Q. X. Mi, E. A. Santori, N. S. Lewis, Chem. Rev. 110, 6446 (2010); https://doi.org/10.1021/cr1002326

[2] F. Bonaccorso, L. Colombo, G. H. Yu, M. Stoller, V. Tozzini, A. C. Ferrari, R. S. Ruoff, V.

Pellegrini, Science 347, 10 (2015); https://doi.org/10.1126/science.1246501

[3] M. Yuan, Z. Sun, H. Yang, D. Wang, Q. Liu, C. Nan, H. Li, G. Sun, S. Chen, Energy Environ. Mater. 6, e122 (2023); https://doi.org/10.1002/eem2.12258

[4] R. D. Cortright, R. R. Davda, J. A. Dumesic, Nature 418, 964 (2002); https://doi.org/10.1038/nature01009

[5] A. A. Gewirth, M. S. Thorum, Inorg. Chem. 49, 3557 (2010); https://doi.org/10.1021/ic9022486

[6] Y. Jiao, Y. Zheng, M. Jaroniec, S. Z. Qiao, Chem. Soc. Rev. 44, 2060 (2015). https://doi.org/10.1039/C4CS00470A

[7] Z. Peng, D. Jia, A. M. Al-Enizi, A. A. Elzatahry, G. Zheng, Adv. Energy Mater. 5, 1402031 (2015); https://doi.org/10.1002/aenm.201402031

[8] C.-T. Dinh, A. Jain, F. P. G. de Arquer, P. De Luna, J. Li, N. Wang, X. Zheng, J. Cai, B. Z. Gregory, O. Voznyy, B. Zhang, M. Liu, D. Sinton, E. J. Crumlin, E. H. Sargent, Nat. Energy, 4, 107 (2019); https://doi.org/10.1038/s41560-018-0296-8

[9] D. Strmcnik, P. P. Lopes, B. Genorio, V. R. Stamenkovic, N. M. Markovic, Nano Energy 29, 29 (2016); https://doi.org/10.1016/j.nanoen.2016.04.017

[10] Y. Cheng, S. Lu, F. Liao, L. Liu, Y. Li, M. Shao, Adv. Funct. Mater. 27, 1700359 (2017); https://doi.org/10.1002/adfm.201700359

[11] T. F. Jaramillo, K. P. Jørgensen, J. Bonde, J. H. Nielsen, S. Horch, I. Chorkendorff, Science 317, 100 (2007); https://doi.org/10.1126/science.1141483

[12] B. Hinnemann, P. G. Moses, J. Bonde, K. P. Jørgensen, J. H. Nielsen, S. Horch, I. Chorkendorff, J. K. Nørskov, J. Am. Chem. Soc. 127, 5308 (2005); https://doi.org/10.1021/ja0504690

[13] A. M. Appel, D. L. DuBois, M. R. DuBois, J. Am. Chem. Soc. 127, 12717 (2005); https://doi.org/10.1021/ja054034o

[14] L. Yang, P. Liu, J. Li, B. Xiang, Catalysts 7, 285 (2017); https://doi.org/10.3390/catal7100285

[15] S. Manzeli, D. Ovchinnikov, D. Pasquier, O. V. Yazyev, A. Kis, Nat. Rev. Mater. 2, 17033 (2017); https://doi.org/10.1038/natrevmats.2017.33

[16] C. Tan, H. Zhang, Chem. Soc. Rev. 44, 2713 (2015); https://doi.org/10.1039/C4CS00182F

[17] R. Ganatra, Q. Zhang, ACS Nano 8, 4074 (2014); https://doi.org/10.1021/nn405938z

[18] M. Chhowalla, H. S. Shin, G. Eda, L.-J. Li, K. P. Loh, H. Zhang, Nat. Chem. 5, 263 (2013); https://doi.org/10.1038/nchem.1589

[19] Z. W. Seh, J. Kibsgaard, C. F. Dickens, I. Chorkendorff, J. K. Nørskov, T. J. Jaramillo, Science 355, 146 (2017); https://doi.org/10.1126/science.aad4998

[20] D. Merki, S. Fierro, H. Vrubel, X. Hu, Chem. Sci. 2, 1262 (2011); https://doi.org/10.1039/C1SC00117E

[21] J. Xie, H. Zhang, S. Li, R. Wang, X. Sun, M. Zhou, J. Zhou, X. W. Lou (David), Y. Xie, Adv. Mater. 25, 5807 (2013); https://doi.org/10.1002/adma.201302685

[22] J. Xie, J. Zhang, S. Li, F. Grote, X. Zhang, H. Zhang, R. Wang, Y. Lei, B. Pan, Y. Xie, J. Am. Chem. Soc. 135, 17881 (2013); https://doi.org/10.1021/ja408329q

[23] J. Shi, D. Ma, G.-F. Han, Y. Zhang, Q. Ji, T. Gao, J. Sun, X. Song, C. Li, Y. Zhang, X.-Y. Lang, Y. Zhang, Z. Liu, ACS Nano 8, 10196 (2014); https://doi.org/10.1021/nn503211t

[24] L. Yang, H. Hong, Q. Fu, Y. Huang, J. Zhang, X. Cui, Z. Fan, K. Liu, B. Xiang, ACS Nano 9, 6478 (2015); https://doi.org/10.1021/acsnano.5b02188

[25] D. Kong, H. Wang, J. J. Cha, M. Pasta, J. Koski, J. Yao, Y. Cui, Nano Lett. 13, 1341 (2013); https://doi.org/10.1021/nl400258t

[26] J. Kibsgaard, Z. Chen, B. N. Reinecke, T. F. Jaramillo, Nat. Mater. 11, 963 (2012); https://doi.org/10.1038/nmat3439

[27] Q. Tang, D. Jiang, Chem. Mater. 27, 3743 (2015); https://doi.org/10.1515/forum-2013-0196

[28] G. Chen, W. F. Dong, B. L. Li, Y. H. Deng, X. H. Wang, X. F. Zhang, H. Q. Luo, N. B. Li, Electrochim. Acta 276, 81 (2018); https://doi.org/10.1016/j.electacta.2018.04.163

[29] D. Kim, D. Sun, W. Lu, Z. Cheng, Y. Zhu, D. Le, T. S. Rahman, L. Bartels, Langmuir 27, 11650 (2011); https://doi.org/10.1021/la201878f

[30] L. Yang, R. Li, Q. Wang, M. Chen, X. Yuan, Chem. Phys. Lett. 749, 137438 (2020); https://doi.org/10.1016/j.cplett.2020.137438

[31] Y. Zheng, J. Rong, J. Xu, Y. Zhu, T. Zhang, D. Yang, F. Qiu, Applied Surface Science 563, 150385 (2021); https://doi.org/10.1016/j.apsusc.2021.150385

[32] J. Lin, P. Wang, H. Wang, C. Li, X. Si, J. Qi, J. Cao, Z. Zhong, W. Fei, J. Feng, Adv. Sci. 6, 1900246 (2019); https://doi.org/10.1002/advs.201900246

[33] J. Staszak-Jirkovský, C. D. Malliakas, P. P. Lopes, N. Danilovic, S. S. Kota, K. Chang, B. Genorio, D. Strmcnik, V. R. Stamenkovic, M. G. Kanatzidis, N. M. Markovic, Nat. Mater. 15, 197 (2016); https://doi.org/10.1038/nmat4481

[34] X. Wang, J. Wang, X. Sun, S. Wei, L. Cui, W. Yang, J. Liu, Nano Res. 11, 988 (2018); https://doi.org/10.1007/s12274-017-1711-3

[35] Y. Gong, Z. Liu, A. R. Lupini, G. Shi, J. Lin, S. Najmaei, Z. Lin, A. L. Elías, A. Berkdemir, G. You, H. Terrones, M. Terrones, R. Vajtai, S. T. Pantelides, S. J. Pennycook, J. Lou, W. Zhou, P. M. Ajayan, Nano Lett. 14, 442 (2014); https://doi.org/10.1021/nl4032296